Observations of the Kuroshio's barotropic and baroclinic responses to basin-wide wind forcing

Magdalena Andres,[1] Young-Oh Kwon,[1] and Jiayan Yang[1]

Received 6 December 2010; revised 19 January 2011; accepted 27 January 2011; published 15 April 2011.

[1] Observations show that the Kuroshio in the East China Sea (ECS-Kuroshio) responds to the large-scale wind stress curl field at two time scales. It is argued that these two responses are related to barotropic and baroclinic modes that reach the ECS via different waveguides. Variability in the ECS-Kuroshio is assessed by comparing satellite altimetry, historical hydrography, and the Pacific Decadal Oscillation (PDO) index with the latter used as a proxy for the large-scale wind stress curl forcing. Sea level difference across the ECS-Kuroshio is positively correlated with PDO at zero lag and negatively correlated at 7 year lag. In contrast, pycnocline steepness and PDO are uncorrelated at zero lag and negatively correlated at 7 year lag. These signals in the ECS-Kuroshio, considered together with wind stress curl anomalies in the open ocean, are consistent with a barotropic response to the wind at zero lag. The barotropic response is likely forced in the central North Pacific by wind stress curl anomalies of opposite sign, one of which is centered at ECS latitudes (~27°N) while the other sits further north. This suggests that, in general, the absolute transport at a given latitude is not simply that predicted by the Sverdrup balance along the latitude. This is a consequence of waveguides that can steer the barotropic mode across latitude lines. In contrast, the signals that lag PDO by 7 years are consistent with a baroclinic mode, which represents the ocean's time-integrated response to the wind stress curl along a single latitude band between 24°N and 27°N.

Citation: Andres, M., Y.-O. Kwon, and J. Yang (2011), Observations of the Kuroshio's barotropic and baroclinic responses to basin-wide wind forcing, *J. Geophys. Res.*, *116*, C04011, doi:10.1029/2010JC006863.

1. Introduction

[2] The Kuroshio, the western boundary current of the subtropical North Pacific, forms near the Philippines, flows northward past the coast of Taiwan and enters the East China Sea (ECS) where it flows as the ECS-Kuroshio northeastward along the shelf break (Figure 1a). After exiting the ECS and flowing along the south coast of Japan, the Kuroshio crosses the Izu Ridge, separates from the coast, and becomes a free jet, the Kuroshio Extension.

[3] In an effort to explain this western boundary current's observed variability, this paper investigates the dynamics that control the ocean's response to the basin-wide wind stress curl forcing. In the North Pacific, large-scale interannual to decadal climate variability is apparent. This variability is particularly pronounced in the sea surface temperature, SST [e.g., *Trenberth*, 1990], as represented by the Pacific Decadal Oscillation (PDO) [*Hare*, 1996; *Mantua et al.*, 1997]. PDO is the principal component time series (PC-1) of the leading empirical orthogonal function (EOF) mode of monthly mean SST in the North Pacific with the global monthly mean SST first removed.

[4] A number of studies in the North Pacific have discussed the ocean's lagged response relative to atmospheric forcing. These studies have focused on the ocean's baroclinic response to the large-scale wind stress curl field. For example, changes in thermocline depth and temperature in the western subtropical gyre and the Kuroshio Extension, evaluated using historical hydrography, lag atmospheric forcing by 3–5 years [*Deser et al.*, 1996, 1999; *Miller et al.*, 1998; *Seager et al.*, 2001; *Hanawa and Kamada*, 2001]. Likewise, satellite altimetry data suggest that Kuroshio Extension strength (zonally averaged) lags the PDO and the associated wind stress curl field [*Qiu*, 2003]. The 3 to 5 year delay in the Kuroshio Extension's response to PDO-related wind forcing has been attributed to the slow westward propagation of baroclinic Rossby waves from the central North Pacific where there is a "center of action" in the wind field [e.g., *Deser et al.*, 1999; *Seager et al.*, 2001; *Qiu*, 2003].

[5] In contrast, observations reported thus far for the North Pacific marginal seas suggest no lag between variability there and the PDO. PDO correlates at zero lag with sea surface height (SSH) both in the ECS and in the Japan/East Sea [*Gordon and Giulivi*, 2004; *Han and Huang*, 2008]. In addition, along-track satellite altimetry together with in situ observations from instruments deployed in the ECS for 23 months along a repeat hydrographic section (the PN line) crossing the Kuroshio (Figure 1a, gray line) suggest that yearly mean transport correlates positively with PDO at zero

[1]Department of Physical Oceanography, Woods Hole Oceanographic Institution, Woods Hole, Massachusetts, USA.

0148-0227/11/2010JC006863

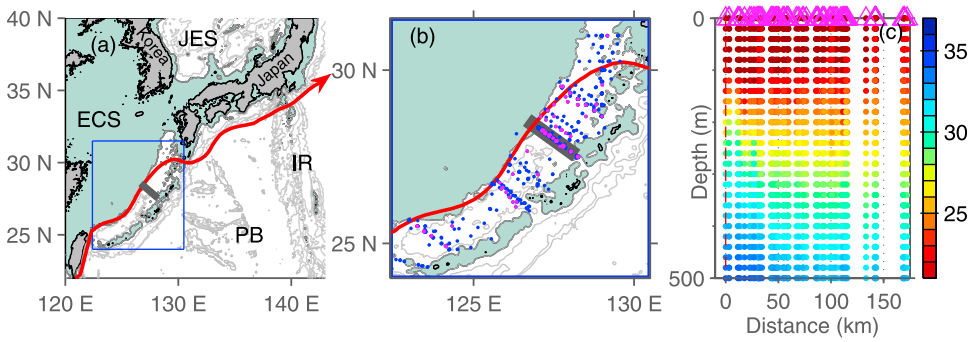

Figure 1. (a) Map of the western North Pacific. The East China Sea (ECS), Japan/East Sea (JES), Philippine Basin (PB), and Izu Ridge (IR) are labeled. Blue square denotes area detailed in Figure 1b. (b) Map of the Okinawa Trough region showing locations of historical hydrography from 1986 to 2008 (dots) with those from 1987 highlighted in magenta. Bathymetry is contoured (light gray lines) at 500 m interval to 3500 m depth. Regions shallower than 500 m are shaded (green). Red contour represents the mean onshore edge of the Kuroshio based on the satellite altimetry. Dark gray segment denotes the PN line. (c) Available hydrographic density profiles as a function of distance from the ECS-Kuroshio's onshore edge for the 1987 casts highlighted in Figure 1b. Colors indicate σ_θ in kg/m^3.

lag with a correlation (r) of 0.76 for 1993–2007 (Figure 2 and the work of *Andres et al.* [2008a, 2009]). These zero lag responses in the marginal seas suggest a barotropic rather than a baroclinic response to forcing over the interior ocean.

[6] According to theory, interannual to decadal transport variability in the Kuroshio there (ECS-Kuroshio) should result from *both* the barotropic and the baroclinic oceanic responses to the large-scale wind stress curl field [*Veronis and Stommel*, 1956]. In the analyses reported here, it is shown that this is indeed the case. Hydrographic data are used in conjunction with satellite altimetry to disentangle the baroclinic and barotropic signals in the ECS. Complementing the previously reported zero lag response in the ECS to remote forcing [*Han and Huang*, 2008; *Andres et al.*, 2009], evidence is presented here of a delayed response in the ECS-Kuroshio to the large-scale wind stress curl field. (Note that at the latitudes of the ECS, based on the Rossby wave speed empirically estimated by *Qiu* [2003], first-mode baroclinic Rossby waves take on the order of 10 years to cross the entire North Pacific basin.) Further, wind stress curl is used to identify the forcing regions for these dynamical modes. It is demonstrated that the barotropic and baroclinic signals that reach the ECS are forced by different parts of the large-scale wind field and arrive in the ECS via propagation along different oceanic waveguides. Such "totally unconnected sources" for the barotropic and baroclinic signals were suggested by *Anderson and Corry* [1985] in their analysis of the Gulf Stream in the Atlantic.

[7] Section 2 presents the data sets used in this study. In section 3, satellite altimetry and historical hydrography are used to demonstrate that the ECS-Kuroshio responds to remote forcing at both a rapid and a delayed time scale. It is argued, in section 4, that these scales are related to barotropic and baroclinic ocean responses, respectively, and their effects on ECS-Kuroshio transport are estimated quantitatively. The connections between the barotropic and baroclinic responses and the wind field are discussed in section 5. Results are summarized in section 6.

2. Data Sets

2.1. Satellite Altimetry

[8] Along-track SSH anomaly data (SLA) from TOPEX/POSEIDON [*Fu et al.*, 1994] followed by Jason-1 and then Jason-2, produced by Ssalto/Duacs and distributed by Aviso with support from Cnes are available at 10 d interval (http://www.aviso.oceanobs.com) with the data corrected for the following: dry and wet troposphere, ionosphere, sea state bias, ocean and pole tides, and a combined atmospheric (including inverse barometer) correction. Aviso's Reference Product is used to assure continuity in the SLA time series. Variability in the sea level difference, ΔSSH, across the ECS-Kuroshio at the PN line is examined using SLA from repeat tracks 138 and 203. ΔSSH values are calculated after *Andres et al.* [2008a] from the difference in SLA between points that lie near the ECS-Kuroshio's offshore edge by the

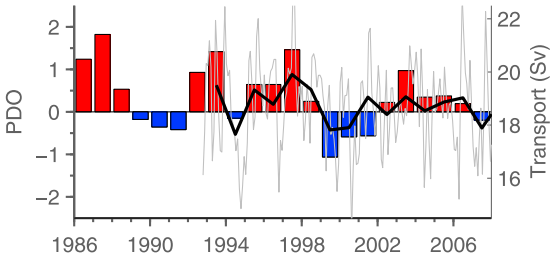

Figure 2. Comparison of yearly mean Pacific Decadal Oscillation (PDO) index (bars) with transport in the ECS-Kuroshio at the PN line (black line, yearly means from the work of *Andres et al.* [2009]; gray line, 40 d low-pass filtered transport from the work of *Andres et al.* [2008a]). At zero lag, r = 0.76 for the 1993–2007 yearly means.

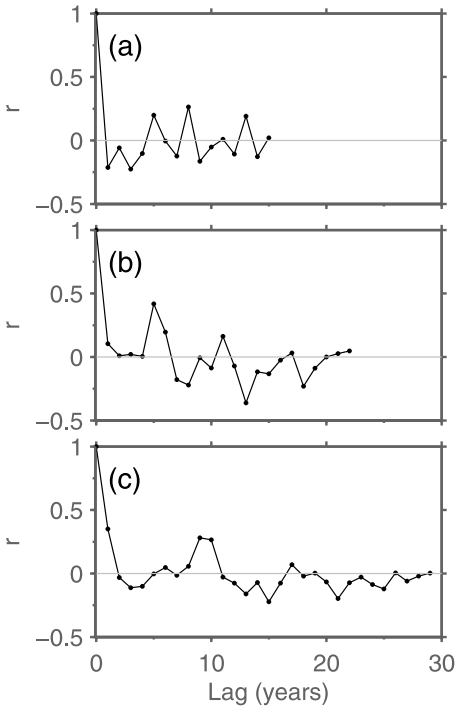

Figure 3. Autocorrelations of (a) Δ sea surface height (ΔSSH), (b) pycnocline steepness, and (c) PDO.

Ryukyu Islands and on its onshore edge at the ECS shelf break (see Figure 1 in the work of *Andres et al.* [2008a]). The separation between these points, L, is 150 km. Annual mean ΔSSH is calculated for 16 years (1993 through 2008) by averaging these SLA differences for each year.

[9] Monthly mean gridded SLA, calculated from multiple satellite missions, are also available from AVISO at 7 d interval. Annual means of these gridded SLA data are used to examine ΔSSH in the broader ECS region.

2.2. Historical Hydrography

[10] Variability in the ECS-Kuroshio's pycnocline steepness is examined with historical hydrography from the Okinawa Trough (Figure 1b). In this part of the ECS, (i.e., between the shelf break and the Ryukyu Islands) pressure, temperature, and salinity data from more than 30 casts per year are available since 1986. Many of these casts were taken along the PN line, which is sampled 4 times per year by the Japan Meteorological Agency. Density, ρ, is thermally controlled in this region, so the analyses reported here are equally valid for the thermocline variability.

2.3. PDO Index and Wind Stress Curl Anomalies

[11] The PDO index is used as a proxy for the variability of the basin-scale wind forcing. The annual mean PDO time series is available from http://jisao.washington.edu/pdo/. It is calculated from EOF analysis of the monthly mean SST in the North Pacific (north of 20°N) from which the globally averaged monthly mean SST has been removed. Annual mean PDO is well-correlated with the PC-1 of annual mean North Pacific wind stress curl, especially for the last few decades [*Qiu*, 2003]. The 1993–2008 correlation, r, between the PC-1 of the wind stress curl and PDO is 0.53. The correlation between PDO and wind stress curl is discussed further in section 5 where the PDO (PC-1 of the SST) is compared with PC-1 of the wind stress curl.

[12] Even though the PDO index is an ocean index, two attributes motivate its use as a forcing proxy in our analyses. First, PDO integrates the influence of the overlying wind field spatially and (in the case of the ocean's baroclinic response) also temporally. Since these integrated effects are reflected both in the PDO and in ECS-Kuroshio variability, it is reasonable for example, that PDO and ΔSSH are better correlated (0.63) than are the wind stress curl PC-1 and ΔSSH (0.53). Second, there is a growing body of work that discusses ocean variability in the context of the PDO [e.g., *Gordon and Giulivi*, 2004; *Qiu et al.*, 2007a; *Han and Huang*, 2008; *Andres et al.*, 2009]. The use of PDO as a forcing proxy here allows for easier comparison of our results with these other works. PDO's limitation, however, is that it reflects the ocean's response to forcing rather than representing the forcing directly. In order to develop the dynamical connection between the atmospheric forcing and the oceanic responses in the ECS, one must consider the wind field directly. This is done in section 5 using wind stress from National Centers for Environmental Prediction–National Center for Atmospheric Research (NCEP-NCAR) reanalysis I (hereafter NCEP wind stress). Wind stress reanalysis data are available at ~2° horizontal resolution and 6 h interval from http://www.esrl.noaa.gov/psd/ provided by NOAA/OAR/ESRL PSD, Boulder, Colorado, USA. These data are used here to construct annual mean wind stress curl anomalies.

2.4. Statistics

[13] In the subsequent sections, correlations of ΔSSH and pycnocline steepness with PDO are discussed. Two points about the statistics warrant comment. First, the lagged correlations are one-sided, with PDO leading. This use of one-sided lagged correlations is motivated both by physics and statistics. Since PDO is being regarded here as a proxy for forcing, it is expected to lead (or be coincident with) variability in the ECS. Since the PDO record extends back to 1900, the one-sided correlation calculations always involve 16 yearly data points for ΔSSH and 23 for pycnocline steepness, independent of lag. Hence, the associated significance thresholds are also independent of lag. Second, significance levels are calculated here by treating each of the data points in the ΔSSH and pycnocline steepness time series as independent realizations. This is reasonable since the autocorrelations of ΔSSH and pycnocline steepness are negligible already at 1 year lag (Figures 3a and 3b). For the 30 year piece of the PDO time series used in this analysis, PDO also has a relatively short correlation length scale (<2 years) (Figure 3c).

3. Rapid and Delayed Responses Observed in the ECS-Kuroshio

3.1. Sea Surface Height

[14] Annual mean ΔSSH across the ECS-Kuroshio at the PN line from 1993 to 2008 is compared with PDO, the forcing proxy, using lagged correlations (Figure 4a). The most significant peak occurs at zero lag ($r = 0.63$, significant at the 99% confidence level). Positive PDO is correlated

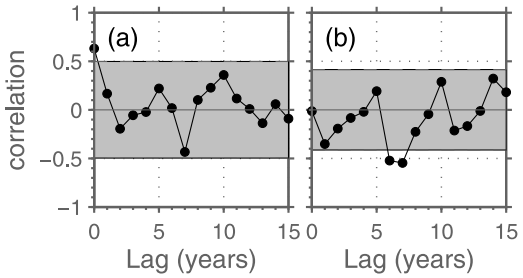

Figure 4. Lagged correlation of yearly mean PDO with (a) ΔSSH and (b) pycnocline steepness across the ECS-Kuroshio (note that a less steep pycnocline is equivalent to an increase in pycnocline slope since this becomes less negative). Positive lag indicates that PDO leads. Correlations outside of the shaded regions are significant at better than the 95% confidence level.

with an increase in ΔSSH, consistent with the findings reported by *Andres et al.* [2009].

[15] The second most significant peak in the lagged correlation ($r = -0.43$) occurs at 7 year lag, though this peak is significant at only the 90% confidence level. An increase in PDO is followed 7 years later by a decrease in ΔSSH. Since the PDO autocorrelation for this time period (Figure 3c) does not have a peak at 7 years, this peak in the lagged correlation is not due to 3–4 year periodicity in PDO. Rather, it likely results from a delayed response of the ECS-Kuroshio to PDO-related wind forcing.

[16] Bearing in mind the two most significant peaks in the lagged correlation, a composite index, $\Delta SSH^*(t)$, is calculated. This index is used to determine how much of the total ΔSSH variance can be attributed to the combined effects of the present year's forcing, $PDO(t)$, and forcing from a previous year, $PDO(t-\tau)$. This is calculated as follows:

$$\Delta\mathrm{SSH}^*(\mathrm{t}) = \alpha\ \mathrm{PDO}(\mathrm{t}) + \beta\ \mathrm{PDO}(\mathrm{t}-\tau) \qquad (1)$$

Here α and β are weighting functions and τ is the time lag in years. The parameters α, β, and τ, are optimized by finding those values that maximize the correlation of ΔSSH^* with ΔSSH. This maximum correlation occurs when $\alpha = 0.3$, $\beta = -0.2$ (which suggests that the present and delayed responses of the ECS-Kuroshio to the wind are of opposite sign but roughly equal magnitude) and $\tau = 7$ (which is consistent with the timing of peaks in the lagged correlation plot). For these parameter values the correlation between ΔSSH^* and ΔSSH is 0.78. This is stronger than the individual zero lag (0.63) and 7 year lag (−0.43) correlations of PDO with ΔSSH. This suggests that variability in the sea surface slope across the ECS-Kuroshio indeed involves two response time scales.

[17] This variability in ΔSSH across the ECS-Kuroshio at the PN line is part of a broader regional signal as can be seen with satellite gridded-SLA. Figure 5 shows correlation maps of PDO with gridded SLA at zero lag and at 7 year lag. The zero-lag map (Figure 5a) shows two noteworthy features: (1) a band of negative correlation that stretches along the entire onshore edge of the ECS-Kuroshio and (2) a weaker positive correlation that stretches along the offshore side. These features combine to give the positive (zero lag) PDO-ΔSSH correlation in the along-track satellite data from the PN line noted above. At 7 year lag (Figure 5b) the correlation pattern is reversed. In this case, the negative PDO-ΔSSH correlation at the PN line results largely from the SLA along the offshore side of the ECS-Kuroshio and less so from the positive correlation along the onshore side.

3.2. Pycnocline Depth

[18] In addition to information about the sea surface obtained from satellite data, as described above, one can use hydrography to elucidate the associated pycnocline variability in the ECS-Kuroshio. Historical hydrography from the Okinawa Trough region (Figure 1b, dots) is used to calculate the 23 year time series (1986–2008) of the annual mean pycnocline steepness across the ECS-Kuroshio as follows. For each cast, the distance from the onshore edge of the ECS-Kuroshio, x, is determined. This onshore edge is taken as the 230 cm contour from the mean (2002–2004) gridded absolute dynamic topography from AVISO satellite altimetry (Figures 1a and 1b, red line). Next, by plotting density profiles of individual casts as a function of x, all casts from a given year are collapsed onto a single cross section regardless of along-Kuroshio distance (e.g., the 110 magenta dots in Figure 1b are all casts from 1987 and their individual density profiles are collapsed onto a single cross section in Figure 1c). This section is smoothed along isopycnals by spline-fitting depth as a function of x to create a yearly mean density section. From this section, the average slope of the 26.5-σ_θ isopycnal between $x = 35$ km and $x = 140$ km is calculated. The magnitude of this slope is the yearly mean pycnocline steepness. (As is typical of western boundary currents, the mean pycnocline slope in the ECS-Kuroshio is negative since its depth increases in the offshore direction, while the steepness is positive absolute of the slope.) This procedure is repeated for each year from 1986 through 2008. The overall 23 year mean cross section is shown for reference in Figure 6a with the 26.5-σ_θ isopycnal highlighted.

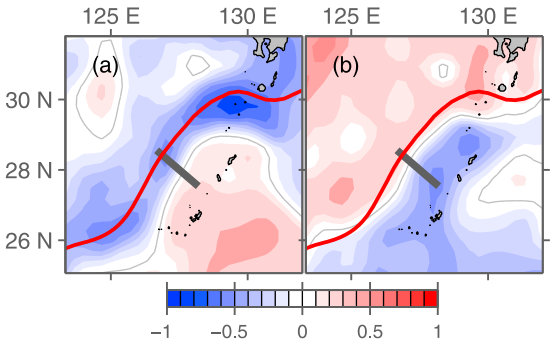

Figure 5. (a) Comparison of the yearly mean SSH anomaly data (SLA) (1993–2008) at each location with yearly mean PDO with a zero-lag correlation map. Grey line is the zero-correlation contour and the contour interval is 0.1. Areas with $|r| > 0.5$ (0.4) are significant at the 95% (90%) confidence level. Dark gray segment is the PN line. Red contour represents the mean onshore edge of the Kuroshio. (b) As in Figure 5a but with SLA lagging PDO by 7 years.

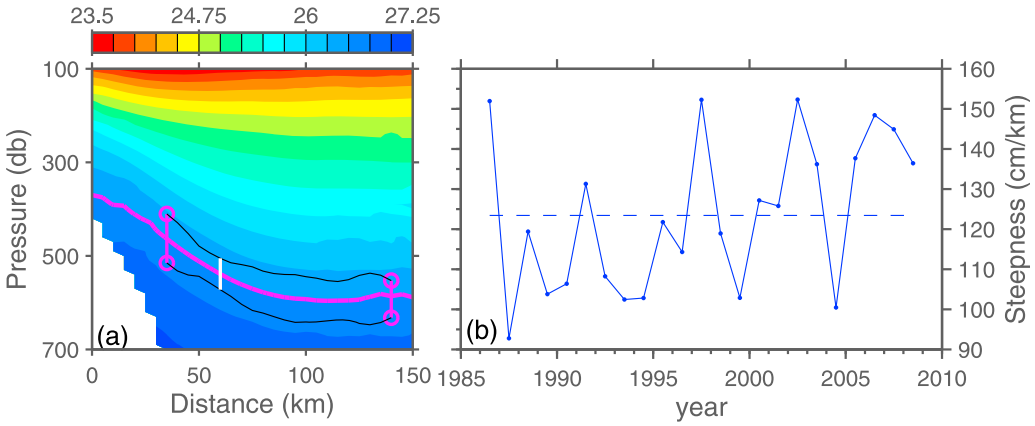

Figure 6. (a) The overall mean σ_θ-profile for 1986–2008 for the upper 700 m of the water column. Contour interval is 0.25 kg/m^3. The 26.5-σ_θ isopycnal, which is used to define the pycnocline, is highlighted in magenta. Black lines indicate the range of this isopycnal's depth as exhibited in the individual yearly mean σ_θ cross sections, with the white line highlighting the minimum in range which occurs at x = 60 km. (b) The time series of the annual mean pycnocline steepness.

[19] The ECS-Kuroshio's annual mean pycnocline steepness (Figure 6b) varies from about 90 cm/km to 150 cm/km, with an overall average of 120 cm/km. The offshore edge of the pycnocline tends to shoal as the onshore side deepens and vice versa. This is demonstrated by the negative correlation (r = −0.40) of the depth of the 26.5-σ_θ isopycnal, $D_{26.5}$, at the onshore side of the ECS-Kuroshio (x = 35 km) and the offshore side (x = 140 km). Further, there is a minimum in the variance and range of $D_{26.5}$ at x = 60 km (the range at x = 60 km is indicated by the white line in Figure 6a), which suggests that this position acts as a pivot point for tilting of the pycnocline.

[20] Pycnocline steepness is compared to PDO by computing lagged correlations (Figure 4b). Notably, there is no correlation at zero lag, suggesting that the annual mean pycnocline steepness is independent of the concurrent annual mean wind forcing (in contrast to the ΔSSH discussed in section 3.1). The most significant peak occurs at 7 year lag, where r = −0.56, significant at the 99% confidence level. If the analysis is performed for the steepness of the 9.5°C isotherm, rather than the 26.5-σ_θ isopycnal, r = −0.60. Higher PDO is followed 7 years later by a less steep pycnocline (and thermocline).

[21] In summary, satellite altimetry and the hydrographic data show that at zero lag only ΔSSH correlates with PDO. In contrast, at 7 year lag, ΔSSH and pycnocline steepness are both anticorrelated with PDO. This variability is discussed in the context of barotropic and baroclinic modes in section 4.

4. Barotropic and Baroclinic Variability in the ECS-Kuroshio

[22] Barotropic variability is characterized by vertically uniform changes in velocity. Accordingly, changes in SSH that are unaccompanied by measureable changes in pycnocline depth (i.e., uncompensated SSH changes) are the hallmark of barotropic variability. In the ECS, the zero-lag correlation of ΔSSH with PDO, taken together with the absence of a zero-lag correlation of pycnocline steepness with PDO, is indicative of such barotropic variability. That this barotropic signature in the ECS occurs at zero lag relative to the PDO is consistent with a fast response to remote forcing. Such fast propagation is typical of barotropic Rossby waves, which can cross the entire Pacific basin in less than a month.

[23] In contrast, baroclinic variability (i.e., variation in vertical shear) is characterized by compensating changes in ΔSSH and pycnocline steepness. In general, the sea surface and the pycnocline are sloped in opposite directions across a western boundary current. So, with x increasing in the offshore direction, the mean sea surface slope ($dSSH/dx$) is positive, the mean pycnocline slope (dD/dx) is negative while the steepness (i.e., $|dD/dx|$) is positive. Vertical shear in a western boundary current increases when the ΔSSH and pycnocline steepness both increase, whereas vertical shear decreases when ΔSSH and the pycnocline steepness both decrease. In the ECS-Kuroshio, the concurrent correlations, at 7 year lag, of both ΔSSH and pycnocline steepness with PDO are consistent with such changes in vertical shear, which typify baroclinic variability. Another characteristic of baroclinic variability, namely that baroclinic Rossby waves propagate much more slowly than the barotropic mode, is also consistent with the ECS observations. The observed 7 year lag between the forcing proxy (PDO) and the responses in the ECS (ΔSSH, pycnocline steepness) is consistent with slow westward propagation by baroclinic Rossby waves from a forcing region to the ECS.

[24] In this section, the independent observations of ΔSSH (from altimetry) and pycnocline steepness (from hydrography) are used jointly to estimate the magnitudes of the zero-lag and 7 year lag variability of the ECS-Kuroshio transport. Treating this western boundary current as a two-layer system with the geostrophic balance holding in each layer, the velocity in the upper layer, v_1, is a function of the pressure gradient, which, in turn, is set by ΔSSH:

$$v_1 = \frac{g}{f}\frac{\Delta SSH}{L} \tag{2}$$

Here g is the acceleration due to gravity, f is the local Coriolis parameter, and L is the width of the current. Lower-layer velocity, v_2, is a function of both the sea surface slope and the interface slope, dD/dx:

$$v_2 = \frac{g}{f}\frac{\Delta SSH}{L} + \frac{g\Delta\rho}{\rho_o f}\frac{dD}{dx} \quad (3)$$

Here $\Delta\rho$ is the density contrast between layers and ρ_o is a mean density (1030 kg/m^3). Then decomposing v_1, v_2, ΔSSH, and dD/dx into mean and time-varying parts, changes in velocity in each layer are related to variability in the sea surface and pycnocline slopes. The ratio of PDO-related changes in lower-layer velocity, v_2', to PDO-related changes in upper-layer velocity v_1', is

$$\frac{v_2'}{v_1'} = 1 + \frac{\Delta\rho}{\rho_o}\frac{(dD/dx)'}{(\Delta SSH/L)'} \quad (4)$$

Here $(dD/dx)'$ is the PDO-related variability in the pycnocline slope, and $(\Delta SSH/L)'$ is the PDO-related variability in the sea surface slope.

[25] To evaluate barotropic variability, $(dD/dx)'$ and $(\Delta SSH/L)'$ in equation (4) are obtained by regressing dD/dx (pycnocline slope) and ΔSSH onto the contemporaneous annual mean PDO, respectively. For dD/dx the regression coefficient is essentially zero, confirming the lack of correlation between pycnocline steepness and PDO discussed in section 3.2. Regressing ΔSSH onto PDO gives $(\Delta SSH/L)' = 0.013$ cm/km. (This is equivalent to a 2.0 cm larger height difference across a 150 km–wide current, per unit increase in PDO.) Since the pycnocline is independent of PDO at zero lag (i.e., $(dD/dx)' = 0$), the last term in equation (4) vanishes and $v_1' = v_2'$. Further, the following is used:

$$v_1' = \frac{g}{f}(\Delta SSH/L)' \quad (5)$$

where $g = 9.8$ m/s^2 and $f = 6.8 \times 10^{-5}$ s^{-1}, giving $v_1' = v_2' = 1.9$ cm/s. For a 150 km–wide current which is ~1000 m deep this corresponds to PDO-related barotropic transport variability which is ~2.8 Sv per unit increase in PDO index. Since annual mean PDO varies between −1.3 and 1.5 during this time period (1993–2008), this barotropic variability represents a 7.7 Sv transport range, which is larger than that shown in Figure 2. This mismatch is discussed in section 6.

[26] To evaluate baroclinic variability, the terms in equation (4) are obtained by performing the regression calculations using 7 year–leading PDO. This gives $(dD/dx)' = 10$ cm/km (equivalent to a 15 m smaller depth difference across the pycnocline across a 150 km–wide current per unit increase in PDO) and $(\Delta SSH/L)' = -0.0082$ cm/km (equivalent to a 1.2 cm smaller height difference across the current per unit increase in PDO). Using these values in equation (5) gives $v_1' = -1.2$ cm/s. Then assuming $\Delta\rho = 2$ kg/m^3, equation (4) gives $v_2' = -1.3 \times v_1' = 1.5$ cm/s. Notably this result ($v_1' \approx -v_2'$) is obtained by combining two completely independent data sources: ΔSSH derived from altimetry and pycnocline steepness derived from hydrography. The ratio v_2'/v_1' does depend on the $\Delta\rho$ assumed in equation (4); to have $v_2'/v_1' = -1$ requires $\Delta\rho = 1.7$ kg/m^3. The water depth here is ~1000 m, so for $\Delta\rho = 1.7$ kg/m^3 the flows are exactly compensated if the pycnocline is 500 m deep. The depth required for compensation increases to 565 m if $\Delta\rho = 2$ kg/m^3. A pycnocline at 400 m depth requires $\Delta\rho = 1.4$ kg/m^3 for perfect compensation. To first order, these values (~1000 m total water depth, ~500 m pycnocline depth, and ~2 kg/m^3 $\Delta\rho$) are representative for the ECS-Kuroshio (Figure 6a), so the velocity increase in one layer is approximately counteracted by the decrease in the other layer and there is little change in net transport, simply a redistribution of it in the vertical. This compensating change is typical of baroclinic variability.

[27] In summary, observations suggest that an increase in PDO is accompanied by an immediate, barotropic (vertically uniform), increase in ECS-Kuroshio velocity and net transport (shown schematically from Figures 7a to 7b). Seven years later this is followed by a baroclinic (vertically sheared) response in which a decrease in upper layer velocity is largely compensated by an increase in lower-layer velocity so that net transport remains essentially unchanged (shown schematically from Figures 7b to 7c).

[28] A consequence of this interplay of baroclinic and barotropic variability along the western boundary is that there is a mean circulation in the lower layer (i.e., in the layer between the pycnocline and the seafloor). This is consistent with previous in situ observations which show that there is no level-of-no-motion beneath the ECS-Kuroshio [*Andres et al.*, 2008b]. Further, since variability in both layers along the western boundary is related to PDO-type forcing, even the bottom layer here is "wind driven."

[29] The redistribution of transport in the vertical by the arrival of a baroclinic Rossby wave after flow has been initially established by a barotropic Rossby wave evokes the ocean spin-up model of *Anderson and Gill* [1975]. However, there are two important differences between the ECS observations and this model. The first difference is that *Anderson and Gill* considered the ocean's approach to steady state with constant wind forcing. In their model, steady state is achieved when the upper layer is intensified and the lower layer shut down by the passage of the baroclinic Rossby wave (shown schematically from Figures 7b to 7d). In contrast, in the North Pacific (where ECS observations show that the lower layer is intensified with the arrival of a baroclinic Rossby wave) the PDO-like forcing is time varying. The second essential difference between the *Anderson and Gill* model and our observations is that the former considered a flat ocean in which barotropic and baroclinic waveguides coincide. In section 5 we argue that the observed variability in the ECS arises precisely because the barotropic and baroclinic signals have arrived in the ECS via different waveguides and from different forcing regions in the North Pacific. Because of this, the absolute transport of the western boundary current at a given latitude is not simply related to the zonally integrated wind stress curl over the interior (i.e., the Sverdrup balance) at that latitude.

5. Wind-Forced Rossby Waves

[30] Thus far, barotropic and baroclinic modes of variability have been identified in the observations by using PDO as a proxy for the large-scale wind forcing. This section begins with a brief examination of the large-scale wind stress curl field and its link to the PDO. Then the two modes of variability are each compared directly to the large-

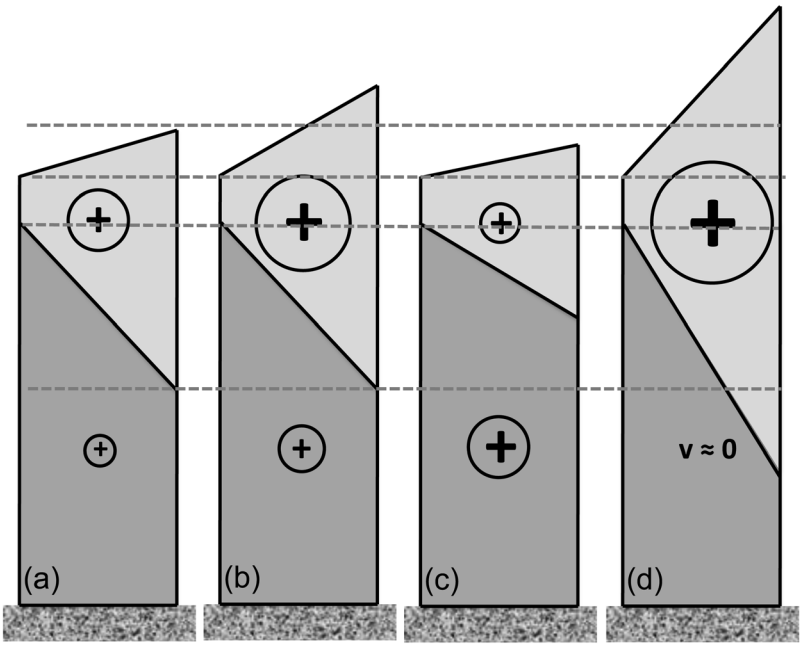

Figure 7. Schematic of a two-layer ECS-Kuroshio responding to the forcing associated with an increase in PDO. (a) The mean ECS-Kuroshio current with a surface-intensified flow. (b) The current's zero-lag response to an increase in PDO: ΔSSH increases while pycnocline slope remains unchanged causing increased velocity in both layers (i.e., a barotropic change). (c) The current's 7 year lagged response in which both the sea surface and pycnocline relax (relative to Figure 7b) such that the upper-layer velocity decreases but the lower-layer velocity increases because of less compensation. (d) The intensification of the upper layer and shut down of the lower layer (relative to Figure 7b) that would be expected for a flat bottom ocean following the barotropic increase in Figure 7b once the baroclinic wave arrives. Note the sea surface and pycnocline slopes are not drawn to scale: changes in ΔSSH across a current are O (1 cm) while changes in pycnocline slope are O (10 m).

scale wind stress curl field in order to (1) identify the specific forcing regions and (2) elucidate the relevant dynamics underlying each mode.

[31] For reference, the zero contour of the mean (1993–2008) wind stress curl is shown in Figure 8b (black line). Figure 8b also shows the loading pattern of the first-mode EOF of the annual mean wind stress curl (shading). The associated PC-1 time series is shown in Figure 8c. In the loading pattern, the wind stress curl over much of the basin is positive between ~35°N and ~40°N. South of 35°N, the wind stress curl in the western part of the basin (i.e., west of ~160°W) is largely negative while to the east it is mainly positive. EOF-1 describes 19% of the variance in the annual mean wind stress curl field. As has been noted previously [e.g., *Qiu*, 2003], the wind stress curl's PC-1 is positively correlated with PDO (r = 0.53); this can be seen from the good agreement in the two time series (Figure 8c, PC-1, black line and PDO, gray line). So, broadly speaking, simultaneously with an increase in PDO, east of ~160°E the zero-wind stress curl line becomes more zonal (rather than trending toward the northeast as it does in the mean). Further, the region of negative curl west of ~160°W gets intensified. So when PDO increases, the wind stress curl along most of 37°N becomes less negative while along 25°N it becomes more negative west of ~160°W.

[32] In the following sections (5.1 and 5.2), to identify the specific forcing regions, the wind stress curl at each latitude is examined separately. Since barotropic waves propagate rapidly, it is appropriate to use the coincident wind stress curl field along a given latitude band to calculate a zonally averaged curl (particularly when considering the ocean's annual mean response to the wind stress curl). Baroclinic waves on the other hand, can take years to cross the basin, and this crossing time must be accounted for when calculating a zonally integrated wind stress curl.

5.1. Barotropic Rossby Waves

[33] The zero-lag correlation between PDO and ΔSSH discussed in section 3.1 suggests that the barotropic mode accounts for about 40% of the observed ΔSSH variability across the ECS-Kuroshio. To identify the specific region(s) where this mode is forced, the zonally averaged annual mean wind stress curl anomaly, $\langle \nabla \times \tau' \rangle$, is calculated as a function of latitude. Then the zero-lag correlation between $\langle \nabla \times \tau' \rangle$ and ΔSSH is calculated for each latitude (Figure 8a). There are two latitude bands where the correlations exceed the 95% significance level. One band (35°N–37°N) lies north of the ECS-Kuroshio (and slightly north of the Kuroshio Extension). Here $\langle \nabla \times \tau' \rangle$ is positively correlated with ΔSSH. If the 85% significance level is used as a threshold, this area of positive correlation is somewhat broader and reaches from 35°N to 47°N. This area of less significant positive correlation is coincident with the region where wind stress curl in the loading pattern (Figure 8b) is positive

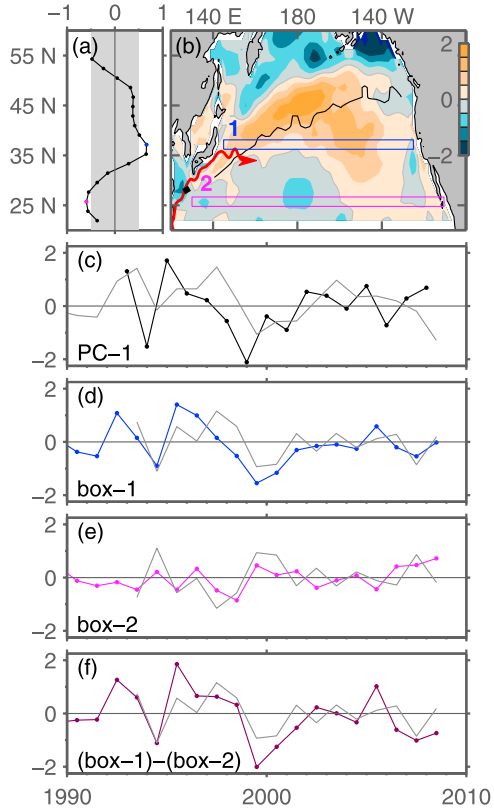

Figure 8. (a) Zero-lag correlations of $\langle \nabla \times \tau' \rangle$ for different latitudes with ΔSSH at the PN line. Regions outside of the shaded area are significant at better than the 95% confidence level. (b) The spatial pattern of the first mode empirical orthogonal function (EOF) of annual mean $\nabla \times \tau$ for 1993–2008 with a contour interval of 0.5×10^{-8} N/m^3. Also shown are the mean (1993–2008) zero wind stress curl line (black), ECS-Kuroshio path (red) and PN line (back square). (c) The associated PC-1 time series (black) with PDO for reference (gray). (d) The normalized time series of $\nabla \times \tau'$ integrated along 37°N (blue, box 1 in Figure 8b) with ΔSSH at the PN line for reference (gray). (e) As in Figure 8d but for 26°N (magenta, box 2 in Figure 8b) with −ΔSSH at the PN line for reference (gray). (f) Normalized $\langle \nabla \times \tau' \rangle$ from 37°N minus $\langle \nabla \times \tau' \rangle$ from 26°N with ΔSSH at the PN line shown for reference (gray).

across most, but not all, of the basin. The band from 35°N–37°N is where the loading pattern is positive across the entire basin; perhaps this is why the positive correlation peaks in this narrow band. The second band (24°N–28°N) is almost at the same latitude as the PN line. (It is centered slightly south of the PN line, but this may be due to limitations of the NCEP wind product which is available at ~2° resolution.) In this band, the correlation is negative. Time series of $\langle \nabla \times \tau' \rangle$ are shown in Figures 8d and 8e for those latitudes with the peak correlations (37.14°N and 25.71°N, respectively). The dynamics that relate North Pacific forcing ($\langle \nabla \times \tau' \rangle$) to the ECS responses (ΔSSH and pycnocline slope) and lead to these observed correlations are considered next.

[34] The positive zero-lag correlation ($r = 0.63$, significant at the 99% confidence level) between ΔSSH and $\langle \nabla \times \tau' \rangle$ zonally averaged along 37.14°N (between 125°W and 145°E, box 1 in Figure 8b) suggests the following mechanism. Positive wind stress curl anomaly over box 1 causes anomalously low SSH because of Ekman divergence in the upper layer. This sea surface low arrives at the onshore side of the ECS-Kuroshio, via a coastal waveguide (as described below). This depresses the onshore side of the ECS-Kuroshio, thereby increasing ΔSSH across the current, consistent with the observed positive correlation.

[35] A secondary effect, can also be related to the wind, namely to $\langle \nabla \times \tau' \rangle$ zonally averaged along 25.71°N (between 111°W and 130°E, box 2 in Figure 8b) which is negatively correlated with ΔSSH ($r = -0.54$, significant at the 97% confidence level). This correlation is consistent with the following: a negative wind stress curl anomaly in box 2 causes anomalously high SSH because of Ekman convergence in the upper layer. The sea surface high propagates zonally toward the ECS. Then when this anomaly arrives on the offshore side of the ECS-Kuroshio it contributes to increased ΔSSH.

[36] The correlation ($r = 0.72$, significant at the 99% confidence level) of ΔSSH with the combined effect of $\langle \nabla \times \tau' \rangle$ in these two boxes (i.e., $\langle \nabla \times \tau' \rangle$ from 37°N minus $\langle \nabla \times \tau' \rangle$ from 26°N, shown in Figure 8f), which is greater than two individual correlations, suggests that barotropic transport variability in the ECS-Kuroshio is indeed driven by the combined effect of these wind stress curl anomalies of opposite sign. Hence it seems that the barotropic response in the ECS is not simply related to forcing of the North Pacific at ECS latitudes, but reflects the effects of wind stress curl anomalies propagating to the ECS from further north as well.

[37] This correlation of ΔSSH with the combined effects of $\langle \nabla \times \tau' \rangle$ can be explained with a conceptual model in which oppositely signed SSH anomalies are generated in the ocean interior along 37°N and 26°N. These barotropic waves are dynamically constrained to propagate along potential vorticity (PV) contours, f/H, where f is the Coriolis parameter and H is water depth. PV contours are roughly zonal in the ocean interior, but are deflected first southward and then northward around the Izu Ridge (at ~140°E, see Figure 1) and then finally cross lines of constant latitude along the steep topography of the western boundary (Figure 9a). SSH anomalies arriving at this boundary from the ocean interior are steered southward (toward lower f) and onshore (toward lower H). In general, the further north a wave starts off, the closer to the coast it must travel in this waveguide because of its initial PV value. This is demonstrated by the PV contours in an idealized flat bottom (4000 m deep) ocean with a sloped western boundary (Figures 9b and 9c). Because of this steering by PV contours, the SSH anomalies generated along 37°N can arrive at the onshore (shallow) side of the Kuroshio. In contrast, SSH anomalies generated along 26°N only reach the offshore (deep) side of the Kuroshio before being steered southward. This conceptual model is supported by results from an idealized two-layer numerical model (M. Andres et al., manuscript in preparation, 2011).

[38] In the real ocean, the Okinawa Trough in the ECS is much shallower than the interior Pacific (~1000 m compared with ~4000 m), so the f/H contours from the ocean interior do not extend across the steep eastern flank of the

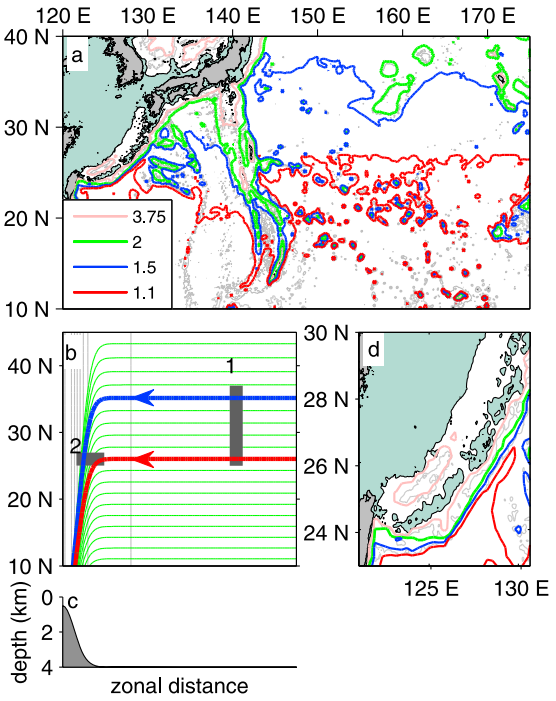

Figure 9. (a) North Pacific potential vorticity (PV) contours (in colors) based on *H* from Smith and Sandwell version 6.2 [*Smith and Sandwell*, 1994]. The 2000 m and 4000 m isobaths are also shown (gray). PV values in the legend have units of 10^{-8} m^{-1} s^{-1}. Green shaded region is shallower than 500 m. (b) PV contours for an idealized ocean basin with the topography profile shown in Figure 9c. The schematic shows how north-south wind stress curl variability in the ocean interior (gray box 1) is converted to east-west SSH variability (gray box 2) along the western boundary as barotropic Rossby waves carry SSH anomalies along *f*/*H* contours to conserve PV. Green lines in Figure 9b are PV contours from 0.7×10^{-8} m^{-1} s^{-1} to 2.5×10^{-8} m^{-1} s^{-1}at 0.1×10^{-8} m^{-1} s^{-1} interval, with the 2.1×10^{-8} m^{-1} s^{-1} and 1.6×10^{-8} m^{-1} s^{-1} contours highlighted in blue and red, respectively. Light gray contours show the topography at 500 m interval. (c) The profile of the bottom topography. (d) A close-up of the ECS and Ryukyu island chain region from Figure 9a.

Ryukyu island chain into the ECS (Figure 9d, see also Figure 64 in *Levitus* [1982] and plate 1 in *Koblinsky* [1990]). However, friction and nonlinearity in regions of strong shear like western boundary currents and atmospheric forcing could push streamlines across *f*/*H* contours so they "leak" into the ECS. While the details of this are not captured by the conceptual model, north-south wind stress curl variability in the ocean interior is translated into cross-isobath SSH variability along the western boundary (Figure 9b) and northern anomalies remain onshore of the southern anomalies, consistent with the observations across the ECS-Kuroshio.

[39] Such a conversion of north-south variability to cross-isobath variability is consistent with regional correlation maps. Figure 10a (see also Figure 5a, for the close-up of the ECS region) shows that PDO is negatively correlated with SSH over much of the ECS shelf (i.e., along the Kuroshio's onshore side) and along the northern flank of the Kuroshio Extension near 35°N. Interestingly, the southern border of this region of negative correlation conforms to the undulations in the mean path (red line) of the Kuroshio Extension where it exhibits quasi-stationary meanders [*Campos and Olson*, 1991]. Further, PDO is positively correlated with SSH along the offshore edge of the ECS-Kuroshio between 24°N and 29°N. A similar pattern, though with slightly weaker correlations, emerges from the analogous correlation of the wind stress curl's PC-1 with SSH (Figure 10b). The similarity of the patterns in Figures 10a and 10b is consistent with the positive correlation of PDO with wind stress curl PC-1.

[40] Note that in both maps, the correlations in the region south of Japan do not follow this pattern of negative correlation on the cyclonic side of the current and positive correlation on the anticyclonic side. The poor correlations here implicate a different process than that depicted in Figure 9. This region, denoted by the dashed Kuroshio path in Figure 10, is where the Kuroshio Large Meander occurs [e.g., *Taft*, 1972]. The dynamics of the Large Meander presumably have a significant effect on SSH there. These dynamics are beyond the scope of this paper, but if their effect on SSH swamps the SSH signal caused by barotropic Rossby waves propagating along the PV contour, the poor correlation in Figure 10 simply represents a low signal-to-noise ratio.

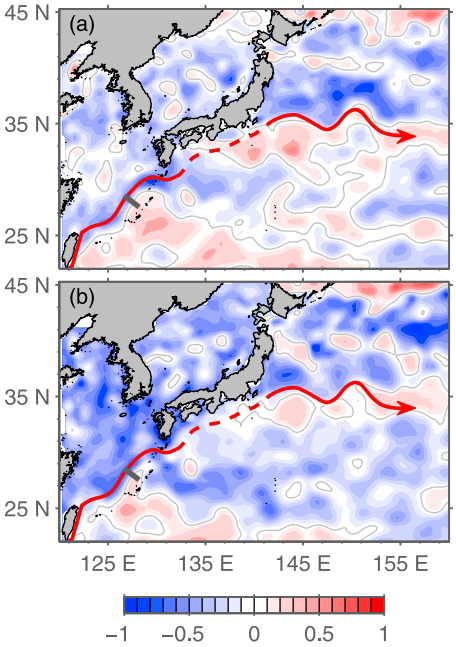

Figure 10. Regional correlation maps. (a) Expanded view of the correlation map shown in Figure 5a comparing the yearly mean SLA (1993–2008) at each location with yearly mean PDO at zero lag. (b) Comparison of the yearly mean SLA (1993–2008) at each location with the wind stress curl PC-1 at zero lag. Contour interval is 0.1. Annotations are as in Figure 5 except here the section of the Kuroshio path that is susceptible the Large Meander is dashed.

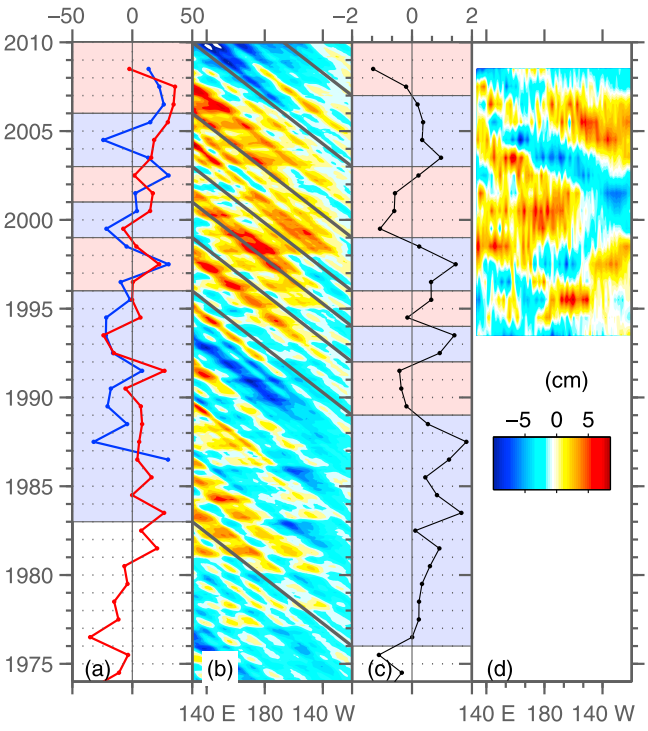

Figure 11. Temporal evolution of the baroclinic signal at ECS latitudes. (a) Comparison of the observed pycnocline steepness anomaly (cm/km) from hydrography (blue line) with normalized $-h'$ from the hindcast with c = 0.5 m/s and $\lambda = 0$ and forced with National Centers for Environmental Prediction (NCEP) winds (red line). Shading highlights the low-frequency changes in PDO shifted by 7 years in comparison with the PDO in Figure 11c connected through the black lines in Figure 11b. (b) A Hovmöller diagram of h' (hindcast). Black lines show propagation at 5 cm/s. (c) The yearly mean PDO index with low-frequency changes highlighted with shading. (d) A Hovmöller diagram of annual mean SSH_{sat} (observed) averaged between 24°N and 27°N.

5.2. Baroclinic Rossby Waves

[41] In contrast to the barotropic mode, baroclinic waves propagate very slowly. At the latitudes of the ECS, baroclinic waves take about 7 years to traverse the 11,000 km distance separating the eastern boundary (~120°W) and the offshore edge of the ECS-Kuroshio (~130°E), assuming a propagation speed of ~5 cm/s (~1600 km/yr). As baroclinic anomalies slowly propagate across the basin, they continually evolve as the ocean integrates the effects of the overlying wind field. At some latitudes in the North Pacific, this process has been successfully represented using a 1 1/2-layer reduced gravity model to hindcast SSH from the wind stress curl field [e.g., *Qiu* 2003; *Qiu et al.*, 2007b; *Qiu and Chen*, 2010]:

$$\frac{\partial h'}{\partial t} - c\frac{\partial h'}{\partial x} = -\frac{g'\nabla \times \tau}{\rho_o g f} - \lambda h' \qquad (6)$$

Here h' is the SSH anomaly, c is the empirically determined speed of the first-mode baroclinic wave, g' is the reduced gravity and λ is a damping coefficient. According to this formulation, h' represents the SSH variability due to propagation and locally forced first-mode baroclinic Rossby waves (i.e., only the baroclinic part, SSH_{bc}, of the total SSH anomalies, SSH_{tot}).

[42] At ECS latitudes, this 1 1/2-layer reduced gravity model does a remarkably poor job of hindcasting the sea surface height anomalies from satellite observations, SSH_{sat}. This is evident in Hovmöller diagrams comparing the hindcast h' propagation from the reduced gravity model with the SSH_{sat} propagation (Figures 11b and 11d).

[43] In light of the significant barotropic contribution (SSH_{bt}) to SSH_{tot} discussed in the previous sections, such poor hindcast skill is not unexpected since the hindcast is based on a formulation which a priori excludes SSH_{bt}. In addition, the model excludes other potential contributions to SSH_{tot} (such as that due to local heat exchange with the atmosphere, SSH_{heat}) while the observed SSH_{sat} shown in Figure 11d includes all of these. Thus, the poor hindcast skill should not be interpreted as evidence against baroclinic Rossby wave propagation through the ocean interior at ECS latitudes. Rather, it supports what has already been proposed in this paper: baroclinic Rossby wave propagation is not the only significant factor controlling SSH (and ΔSSH) at ECS latitudes.

[44] Unlike SSH_{sat}, the pycnocline should not be significantly affected by those processes which control SSH_{bt} or SSH_{heat}. Hence variability in pycnocline depth is a "purer" indicator of the presence of wind-forced baroclinic Rossby waves than is SSH_{sat} variability. With this motivation, equation (5) is revisited, this time considering the variation in the pycnocline depth on the offshore side the ECS-Kuroshio, D'_{off}, keeping in mind that $-h'$ (or equivalently, $-SSH_{bc}$) is proportional to D'_{off}. Equation (5) is integrated from the eastern boundary (100°W) to just offshore of the ECS-Kuroshio (133°E) along the latitude band between 24°N and 27°N. Instead of prescribing c determined from SSH_{sat} [e.g., *Qiu*, 2003], this hindcast is optimized by finding those values of c and λ that maximize the correlation between the hindcast ($-h'$, or equivalently, D'_{off}) and the observed (from historical hydrography) $D_{26.5}$ on the offshore side of the ECS-Kuroshio (i.e., at x = 140 km, see section 3.2). Optimization gives $\lambda = 0$ (no damping) and c = 5.0 cm/s. (Note that this propagation speed is consistent with the empirical estimation of *Qiu* [2003] based on SSH_{sat}.) With these parameters, the correlation between D'_{off} ($-h'$) and the observed $D_{26.5}$ is 0.40 (significant at the 95% confidence level). This correlation suggests that, despite the poor correspondence between Hovmöller diagrams for the observations (SSH_{sat}) and the hindcast (h'), baroclinic Rossby waves *do* propagate zonally at ECS latitudes and their arrival on the offshore side of the ECS-Kuroshio affects the pycnocline depth in this western boundary current.

[45] The interaction of a heaved or depressed pycnocline with the steep topography of the western boundary is beyond the scope of this paper. However, it is noted that the correlation between D'_{off} and $D_{26.5}$ at the onshore side of the ECS-Kuroshio (where x = 35 km) is negative ($r = -0.48$). This suggests that as the offshore edge of the pycnocline is depressed by the arrival of a baroclinic Rossby wave, the onshore side shoals, causing a steeper pycnocline. The result is a strong negative correlation between observed (from hydrography) pycnocline steepness and the hindcast

D'_{off} ($r = -0.53$). This correlation is evident in Figure 11a which shows time series of the observed pycnocline steepness (blue line) and h' ($-D_{off}$) from the wind-forced hindcast (red line).

6. Summary

[46] This analysis began by using an ocean index, namely the PDO, as a proxy for the wind stress curl forcing. Now, after having carefully investigated the direct relationship between ECS-Kuroshio variability and the wind stress curl, we are in a position to examine the following question: why is the PDO such a good proxy for the basin-scale wind stress curl forcing?

[47] PDO integrates the influence of the overlying wind field temporally and spatially (because PDO is calculated from the basin-wide SST field). The ocean's response in its velocity field to the basin-wide wind-forcing consists of the barotropic mode which is a spatial-integrator and the baroclinic mode which is a spatial- and temporal- integrator. This is demonstrated by our preceding analyses which show that barotropic variability in the ECS-Kuroshio is correlated with area-average wind stress curl. Notably, this spatially integrated effect is not just zonal but also involves different latitudes. The slow (relative to atmospheric variability) zonal propagation of baroclinic Rossby waves along the characteristics that span the entire basin results in the spatial and temporal integration of wind forcing. Since waveguides direct these barotropic and baroclinic signals to the ECS, the ECS-Kuroshio acts as a "collector" of the basin-wide wind-forced variability and, like the PDO, reflects the effects of spatial and temporal integration of the wind forcing.

[48] These dynamical modes both contribute to the satellite-measured SSH variability. As has been demonstrated here, in regions with sufficient hydrographic data, such as the ECS, the satellite record can be decomposed into the two modes. Below, the two main results from this decomposition procedure are each summarized and considered in the context of previous studies.

[49] First, on the basis of ECS-Kuroshio observations, the rapidly propagating barotropic response manifests itself in ΔSSH variability that is uncorrelated with changes in pycnocline steepness. This response results from Ekman divergences and convergences driven remotely by wind stress curl anomalies of opposite sign centered at different latitudes. The northern anomaly propagates westward to the boundary and then follows a coastal waveguide to the ECS-Kuroshio's onshore side, whereas the southern anomaly, of opposite sign, propagates through the ocean interior to the current's offshore side.

[50] The net transport change associated with this barotropic variability in the ECS-Kuroshio is almost 8 Sv. This is about one third of the mean transport there [*Ichikawa and Beardsley*, 1993; *Andres et al.*, 2008b] and is ~4 times larger than the net transport change coincident with PDO changes estimated by *Andres et al.* [2009] and shown here in Figure 2. This original estimate of PDO-related transport variability depended implicitly on the following assumption: the proportion of baroclinic to barotropic flow, V_{BC}/V_{BT}, in the ECS-Kuroshio is constant in time and hence, once calibrated with in situ data, ΔSSH_{sat} can be used to infer absolute transport in the underlying water column. This assumption was based on the very strong correlation of a 13 month transport time series (determined from in situ data) with satellite-derived ΔSSH [*Andres et al.*, 2008a]. Processes which control ECS-Kuroshio absolute transport variability at periods shorter than 1 year without changing V_{BC}/V_{BT} might include, for example, arrival of eddies, propagation of frontal waves, or variability induced by local wind forcing. Whatever the exact mechanisms, such variability is ubiquitous in the data from the ECS-Kuroshio. The work here suggests that while high-frequency variability in the ECS-Kuroshio transport does not affect V_{BC}/V_{BT}, processes controlling transport variability at the lower frequencies considered here (where all time series analyzed were yearly means), clearly do not preserve this ratio.

[51] The second result from the decomposition of the ECS-Kuroshio variability is that, in addition to the barotropic mode, a baroclinic signal is present in the observations, with ΔSSH and pycnocline steepness varying concurrently. However, this signal is not a simple Anderson and Gill – type baroclinic counterpart to the above mentioned barotropic response (i.e., it is not a baroclinic signal in which the lower layer is shut down and initial barotropic transport is redistributed into the upper layer). The baroclinic signal is likely due to baroclinic Rossby waves which propagate westward along ECS latitudes at ~5 cm/s from the ocean interior and arrive at the offshore edge of the western boundary current. These baroclinic waves are essentially undamped, so the signal at the offshore side of the ECS-Kuroshio represents the ocean's integrated response to winds blowing over the entire latitude band. The waves' propagation is difficult to identify in SSH_{sat} because of other processes affecting SSH_{tot} (e.g., SSH_{bt}). Nevertheless, evidence for the arrival of baroclinic Rossby waves is present in the pycnocline as elucidated by the hydrographic data. This baroclinic signal does affect the vertical shear, however, net transport remains essentially unchanged because SSH_{bc} variability is compensated by pycnocline depth changes.

[52] In conclusion, the data presented here suggest that the onshore and offshore edges of the ECS-Kuroshio have different sources of variability; transport variability in the ECS-Kuroshio is affected by both. Similar processes may be at work along the western boundary of the North Atlantic where sea level on the onshore side of the Gulf Stream (from tide gage data) is incoherent with that on the offshore side (from a wind-forced model), even at low frequencies [*Sturges and Hong*, 2001]. Barotropic waveguides are set by topography while baroclinic waveguides are not. As a result, the net transport variability at a given latitude is not simply related to the Sverdrup balance at that latitude.

[53] **Acknowledgments.** M.A. was supported by the Postdoctoral Scholar Program at the Woods Hole Oceanographic Institution, with funding provided by the Ocean and Climate Change Institute. Further support was provided to M.A., Y.-O.K., and J.Y. by NSF under grant OCE-1028739. We appreciate the helpful suggestions from three anonymous reviewers.

References

Anderson, D. L. T., and R. A. Corry (1985), Ocean response to low frequency wind forcing with application to the seasonal variation in the Florida Straits–Gulf Stream transport, *Prog. Oceanogr.*, *14*, 7–40, doi:10.1016/0079-6611(85)90003-5.

Anderson, D. T. L., and A. E. Gill (1975), Spin-up of a stratified ocean, with applications to upwelling, *Deep Sea Res.*, *22*, 583–596.

Andres, M., J.-H. Park, M. Wimbush, X.-H. Zhu, K.-I. Chang, and H. Ichikawa (2008a), Study of the Kuroshio/Ryukyu Current system based on satellite-altimeter and in situ measurements, *J. Oceanogr.*, *64*, 937–950, doi:10.1007/s10872-008-0077-2.

Andres, M., M. Wimbush, J.-H. Park, K.-I. Chang, B.-H. Lim, D. R. Watts, H. Ichikawa, and W. J. Teague (2008b), Observations of Kuroshio flow variations in the East China Sea, *J. Geophys. Res.*, *113*, C05013, doi:10.1029/2007JC004200.

Andres, M., J.-H. Park, M. Wimbush, X. Zhu, H. Nakamura, K. Kim, and K.-I. Chang (2009), Manifestation of the Pacific Decadal Oscillation in the Kuroshio, *Geophys. Res. Lett.*, *36*, L16602, doi:10.1029/2009GL039216.

Campos, E. J. D., and D. B. Olson (1991), Stationary Rossby waves in western boundary current extensions, *J. Phys. Oceanogr.*, *21*, 1202–1224, doi:10.1175/1520-0485(1991)021<1202:SRWIWB>2.0.CO;2.

Deser, C., M. A. Alexander, and M. S. Timlin (1996), Upper-ocean thermal variations in the North Pacific during 1970–1991, *J. Clim.*, *9*, 1840–1855, doi:10.1175/1520-0442(1996)009<1840:UOTVIT>2.0.CO;2.

Deser, C., M. A. Alexander, and M. S. Timlin (1999), Evidence for a wind-driven intensification of the Kuroshio Current Extension from the 1970s to the 1980s, *J. Clim.*, *12*, 1697–1706, doi:10.1175/1520-0442(1999)012<1697:EFAWDI>2.0.CO;2.

Fu, L.-L., E. J. Christensen, C. A. Yamarone, M. Lefebvre, Y. Menard, M. Dorrer, and P. Escudier (1994), TOPEX/POSEIDON mission overview, *J. Geophys. Res.*, *99*, 24,369–24,381, doi:10.1029/94JC01761.

Gordon, A. L., and C. F. Giulivi (2004), Pacific decadal oscillation and sea level in the Japan/East Sea, *Deep Sea Res. Part I*, *51*, 653–663, doi:10.1016/j.dsr.2004.02.005.

Han, G., and W. Huang (2008), Pacific decadal oscillation and sea level variability in the Bohai, Yellow, and East China seas, *J. Phys. Oceanogr.*, *38*, 2772–2783, doi:10.1175/2008JPO3885.1.

Hanawa, K., and J. Kamada (2001), Variability of core layer temperature (CLT) of the North Pacific subtropical mode water, *Geophys. Res. Lett.*, *28*, 2229–2232, doi:10.1029/2000GL011716.

Hare, S. R. (1996), Low-frequency climate variability and salmon production, Ph.D. thesis, 306 pp., Univ. of Wash., Seattle, Wash.

Ichikawa, H., and R. C. Beardsley (1993), Temporal and spatial variability of volume transport of the Kuroshio in the East China Sea, *Deep Sea Res. Part I*, *40*, 583–605, doi:10.1016/0967-0637(93)90147-U.

Koblinsky, C. J. (1990), The global distribution of f/H and the barotropic response of the ocean, *J. Geophys. Res.*, *95*, 3213–3218, doi:10.1029/JC095iC03p03213.

Levitus, S. (1982), *Climatological Atlas of the World Ocean*, 173 pp., NOAA, Rockville, Md.

Mantua, N. J., S. R. Hare, Y. Zhang, J. M. Wallace, and R. C. Francis (1997), A Pacific interdecadal climate oscillation with impacts on salmon production, *Bull. Am. Meteorol. Soc.*, *78*, 1069–1079, doi:10.1175/1520-0477(1997)078<1069:APICOW>2.0.CO;2.

Miller, A. J., D. R. Cayan, and W. B. White (1998), A westward-intensified decadal change in the North Pacific thermocline and gyre-scale circulation, *J. Clim.*, *11*, 3112–3127, doi:10.1175/1520-0442(1998)011<3112:AWIDCI>2.0.CO;2.

Qiu, B. (2003), Kuroshio Extension variability and forcing of the Pacific decadal oscillations: Responses and potential feedback, *J. Phys. Oceanogr.*, *33*, 2465–2482, doi:10.1175/2459.1.

Qiu, B., and S. Chen (2010), Interannual-to-decadal variability in the bifurcation of the North Equatorial Current off the Philippines, *J. Phys. Oceanogr.*, *40*, 2525–2538, doi:10.1175/2010JPO4462.1.

Qiu, B., S. Chen, and P. Hacker (2007a), Effect of mesoscale eddies on Subtropical Mode Water variability from the Kuroshio Extension System Study (KESS), *J. Phys. Oceanogr.*, *37*, 982–1000, doi:10.1175/JPO3097.1.

Qiu, B., N. Schneider, and S. Chen (2007b), Coupled decadal variability in the North Pacific: An observationally constrained idealized model, *J. Clim.*, *20*, 3602–3620, doi:10.1175/JCLI4190.1.

Seager, R., Y. Kushnir, N. H. Naik, M. A. Cane, and J. Miller (2001), Wind-driven shifts in the latitude of the Kuroshio-Oyashio Extension and generation of SST anomalies on decadal timescales, *J. Clim.*, *14*, 4249–4265, doi:10.1175/1520-0442(2001)014<4249:WDSITL>2.0.CO;2.

Smith, W. H. F., and D. T. Sandwell (1994), Bathymetric prediction from dense satellite altimetry and sparse shipboard bathymetry, *J. Geophys. Res.*, *99*, 21,803–21,824, doi:10.1029/94JB00988.

Sturges, W., and B. G. Hong (2001), Gulf Stream transport variability at periods of decades, *J. Phys. Oceanogr.*, *31*, 1304–1312, doi:10.1175/1520-0485(2001)031<1304:GSTVAP>2.0.CO;2.

Taft, B. A. (1972), Characteristics of the flow of the Kuroshio south of Japan, in *Kuroshio—Its Physical Aspects*, edited by H. Stommel and K. Yoshida, pp. 165–216, Univ. of Tokyo Press, Tokyo.

Trenberth, K. E. (1990), Recent observed interdecadal climate changes in the Northern Hemisphere, *Bull. Am. Meteorol. Soc.*, *71*, 988–993, doi:10.1175/1520-0477(1990)071<0988:ROICCI>2.0.CO;2.

Veronis, G., and H. Stommel (1956), The action of variable wind stresses on a stratified ocean, *J. Mar. Res.*, *15*, 43–75.

M. Andres, Y.-O. Kwon, and J. Yang, Department of Physical Oceanography, Woods Hole Oceanographic Institution, 266 Woods Hole Rd., MS 21, Woods Hole, MA 02543, USA. (mandres@whoi.edu)